



HAL
open science

Simulating tropical river plumes, a set of parametrizations based on macroscale data: A test case in the Mekong Delta region

R. Hordoir, Nguyen K.D., J. Polcher

► To cite this version:

R. Hordoir, Nguyen K.D., J. Polcher. Simulating tropical river plumes, a set of parametrizations based on macroscale data: A test case in the Mekong Delta region. *Journal of Geophysical Research*, 2006, 111, pp.1-18. 10.1029/2005JC003392 . hal-00203323

HAL Id: hal-00203323

<https://hal.science/hal-00203323>

Submitted on 31 May 2021

HAL is a multi-disciplinary open access archive for the deposit and dissemination of scientific research documents, whether they are published or not. The documents may come from teaching and research institutions in France or abroad, or from public or private research centers.

L'archive ouverte pluridisciplinaire **HAL**, est destinée au dépôt et à la diffusion de documents scientifiques de niveau recherche, publiés ou non, émanant des établissements d'enseignement et de recherche français ou étrangers, des laboratoires publics ou privés.

Copyright

Simulating tropical river plumes, a set of parametrizations based on macroscale data: A test case in the Mekong Delta region

R. Hordoir,¹ K. D. Nguyen,¹ and J. Polcher²

Received 14 November 2005; revised 4 May 2006; accepted 26 May 2006; published 28 September 2006.

[1] A year-long simulation of the Mekong river plume is conducted. The purpose is to identify the main processes impacting the fate of tropical freshwater runoff onto the shelf for later inclusion into a global ocean circulation model. Factors influencing the river plume in a general case are listed and are included in a coastal ocean configuration of the Princeton Ocean Model. This is achieved either explicitly, as for wind forcing, or using parametrizations corresponding to the length and timescales of river plumes physics, as for tides or estuaries. Results exhibit a strong seasonal variability related to the monsoon wind and river flow regimes of the region. A comparison with in situ measurements made during a campaign carried out in 1997 shows a good agreement. Vertical salinity profiles extracted from the model configuration correspond to conductivity-temperature-depth salinity profiles behavior established during the campaign. This model configuration also provides a good estimate of sea surface salinity in the vicinity of the coast of the Mekong Delta.

Citation: Hordoir, R., K. D. Nguyen, and J. Polcher (2006), Simulating tropical river plumes, a set of parametrizations based on macroscale data: A test case in the Mekong Delta region, *J. Geophys. Res.*, *111*, C09036, doi:10.1029/2005JC003392.

1. Introduction

[2] Continental shelves provide about 1.2 sverdrups of freshwater runoff into the global ocean, a major amount of this freshwater being rejected in a latitude stripe included between 20°S and 20°N [Dai and Trenberth, 2002]. From a physical perspective, this flow can be considered as very small compared to ocean currents, but it influences ocean dynamics and physics in coastal regions by the input of low-density water it provides. This is especially true for the world's biggest rivers as shown by Geyer and Kineke [1995], Simpson [1997], or Simpson and Snidvongs [1998]. This contribution must be included in an appropriate way in global circulation models (GCM) when the aim is to model climate variations over long periods and when changes in the water cycle can be expected. Therefore a correct parametrization of global freshwater runoff must be included in ocean GCMs. As a step to reach a global parametrization of freshwater runoff for ocean GCMs we proceed in this paper to the achievement of two tasks.

[3] The first one is an identification and a parametrization of the main processes that shape river plumes in tropical regions. This task is also the basement required to establish a parametrization of tropical runoff for an ocean GCM. It has to be achieved using only data accessible at a global

scale. The second one is a testing task: the parametrizations established are tested on a real case for which a numerical configuration is set. Results are compared with experimental data.

[4] An extensive literature can be found on river plumes: from a numerical point of view, one can cite Kourafalou *et al.* [1996b, 1996a] with a special focus on the South Atlantic Bight. There are also a lot of more conceptual numerical studies using idealized coastal areas, in order, for example, to relate plume extension to river inflow and local parameters [Garvine, 1999]. One can also cite some studies mixing theoretical consideration and numerical experiments, in order, for example, to find the geometry of the freshwater bulge created by the river intrusion [Yankovsky and Chapman, 1997]. Depending on the aim of the study, authors focus on different essential points important for river plume dynamics; Fong and Geyer [2001], for instance, concentrate their study on the interaction of the wind with the plume. There are also papers insisting more on the role of the river mouth configuration, how the width of the mouth and inflow salinity will influence transport in the downshelf baroclinic current [Fong and Geyer, 2001]. A river mouth Rossby number is defined as $R_o = U/fB$ with U standing for velocity of the inflow, f the Coriolis parameter, and B the river width. Fong and Geyer [2001] show that freshwater transport in the coastally trapped baroclinic current depends on the mouth Rossby number, for a given freshwater flow. This latest study completes the work done by Garvine [1995] that relates river plume characteristic to a baroclinic Kelvin number. The main features of the low-density water plume and its interaction with local forcing and parameters will not be explicitly described again as

¹Laboratoire de Morphodynamique Continentale et Côtière, UMR 6143, Université de Caen, Caen, France.

²Laboratoire de Météorologie Dynamique du CNRS, IPSL, CNRS, Paris, France.

readers will find them in papers cited above and in many others [O'Donnel, 1990; Marsaleix *et al.*, 1998; Geyer *et al.*, 2000; García Berdeal *et al.*, 2002]. Whether it be with experimental, numerical or theoretical papers, important processes that will influence river plume dynamics have been identified in the literature.

1.1. River and Estuarine Forcing

[5] If we only consider the forcing imposed by the freshwater flow, the Kelvin number defined by Garvine [1995] gives a key to classify low-density coastal discharges. If it is small, which means the width of the coastal current is small or that the Coriolis acceleration is small, the shape created by the inflow is similar to a jet. Advection effects are the dominant terms of the left hand side of the primary equations. If the Kelvin number is large, then Coriolis momentum becomes dominant and plumes behave like those described by many authors [Chao and Boicourt, 1986; Weaver and Hsieh, 1987; Chao, 1988b; Simpson, 1997]: the inflow of freshwater creates a baroclinic current, coastally trapped and that flows in the direction of propagation of the Kelvin wave. Experiments made by Fong and Geyer [2002] confirm results from Garvine [1995] using a mouth Rossby number. They also show that upstream-of-river-mouth processes will have an impact on the features of the plume. For a given pure freshwater flow, and a given mouth width and depth, estuarine dynamics will influence the fate of freshwater, and especially because of estuarine mixing with sea water that will increase the volumic flow at the mouth, but also increase the salinity of the flow rejected into the ocean. This will affect the river inflow velocity and decrease the baroclinic pressure gradient created by the inflow. Effects over freshwater transport along the coast are explained by Fong and Geyer [2002], who show increase of the anticyclonic bulge size at the vicinity of the mouth, decrease of the freshwater transport in the coastal current. This is coherent with the theory elaborated by Yankovsky and Chapman [1997] as they relate the increase of the size of the bulge with the Froude number, while its basic radius is shown to be proportional to the baroclinic Rossby radius. The depth at which the base of the river plume will be located is also affected by the density and the velocity of the river inflow in the coastal area [Yankovsky and Chapman, 1997]. A strong inflow velocity and a weak baroclinic gradient are likely to create a bottom advected plume, depending on the slope of the bottom. Apart from the simple baroclinic current entering the estuary, estuarine dynamics are influenced by tidal forcing as it provides a major input of mixing in channels. From a horizontal point of view, MacCready [2004] shows that time averaged tidal currents may be considered as a horizontal diffusion. In the meantime, tidal current high-frequency variability within the estuary proves to have little effect on the main features of the plume as shown by Yankovsky *et al.* [2001].

1.2. Local Currents

[6] A baroclinic current is created by the input of freshwater along the coast, but it can interact with local currents. In this survey, we will distinguish two types of local currents.

[7] The first ones are the large-scale currents which variability is much lower than the variability of the river plume. They are currents that will have a major influence on the shape of the river plume as shown by García Berdeal *et al.* [2002]. Working on the Columbia river, García Berdeal *et al.* [2002] have shown that a current opposed to the one created by the plume will destroy the river plume quickly.

[8] The second type of local currents that we will distinguish are the tidal currents. Because of their high variability, such currents have little advective effect on the plume if one looks at the evolution of the plume on a long timescale as shown by Garvine [1999]. Their energy input, however, produces high vertical shear stress that may have an influence on the density stratification created by the input of freshwater: most of the river plume dynamics are created by the strong stratification introduced within the coastal area. This strong stratification creates a baroclinic stream carrying low-density water. Under this baroclinic current flows in the opposite direction a current carrying salted water. The two currents eventually meet in the estuary or in shallow bay areas. Therefore the coastal circulation generated by the inflow of freshwater is stronger in volume and momentum than the inflow of volume and the inflow of momentum brought by the freshwater source. If, however, a process destroys the stratification brought by the river inflow, it will lower the full coastal dynamics and from a general point of view the coastal overturning created by the river inflow. Simpson [1997] provides a lot of references showing the effects of vertical tidal mixing on freshwater plumes, just like vertical tidal mixing has a major influence on density fronts created by temperature gradients as shown by Simpson and Hunter [1974]. Geyer [1995] in his study on the Amazon River has confirmed the importance of tidal mixing far offshore of the river mouth, and even made distinction between spring and neap tides stratification in the Amazon river plume. We believe this to be true for many tropical rivers of the world as they often end their continental journey in regions of sedimental shelves that extend far offshore. Geyer *et al.* [1996] show the extent of a shallow bathymetry far off the coast for the Amazon River, which means high tidal mixing even off the coast.

1.3. Atmospheric Forcing

[9] Wind-forcing is shown to greatly affect plume dynamics. Fong and Geyer [2001] show on a theoretical case that the pycnocline situated at the base of the river plume blocks momentum transmitted by the wind through water surface. The concentration of momentum in a short water column results in the plume to react much stronger to atmospheric wind forcing than would a neighbor water column lacking density stratification. The Ekman transport in the river plume will be stronger. Within the plume, advection velocities will be higher to either advect the plume offshore in the case of an upwelling wind, or compress the plume along the coast resulting in a thin coastal current. García Berdeal *et al.* [2002] arrive at the same result in a study made on the Columbia river plume. Fong *et al.* [1997] show similar results thanks to observations made in the gulf of Maine. Prior to Fong and Geyer [2001] and García Berdeal *et al.* [2002], we can also cite the studies made by Kourafalou *et al.* [1996a] in which wind forcing is included. Some other studies have shown

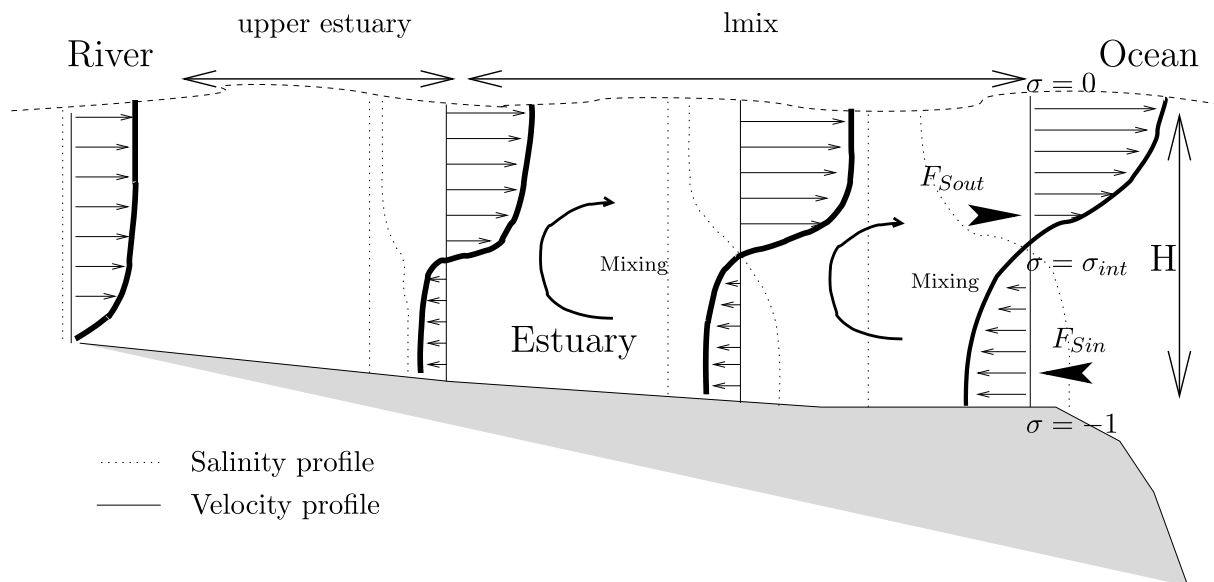


Figure 1. Schematic view of estuarine salinity and velocity profiles.

the influence of wind on the shape of a river plume and one can also cite *Chao [1988a]*, *Masse and Murphy [1990]*, and *Münchow and Garvine [1993]*.

1.4. Purpose of the Study

[10] The estuarine and coastal processes that will model the shape of a tropical river plume will be identified and then parameterized. Moreover, this will be done using data accessible on a global scale, data that could be given to or taken from a GCM, whether it is ocean, continental or atmospheric GCM. Our aim is to obtain realistic results with a local coastal ocean model, and acquire knowledge dealing with river/ocean interaction that could be extended to the global scale.

[11] The article first describes how processes will be parameterized in the model configuration that will be used (section 2). In section 3 the model configuration for the Mekong river plume using the Princeton Ocean Model (POM) [*Blumberg and Mellor, 1987*] is presented. The model configuration is set in the region of freshwater influence of the Mekong Delta in 1997, during which a conductivity-temperature-depth (CTD) campaign has been made in March (dry season) and October (end of the Monsoon) [*Hungspreugs, 1998*]. Numerical results will be commented and compared to experimental results in section 4. In section 5, we will analyze the effects of one of the parametrizations that has been proposed in section 2. Finally, section 6 will conclude this paper.

2. Processes Parametrizations

2.1. Estuarine Mixing

[12] As presented in section 1, estuarine mixing is key to understanding plume features. It is in the estuary that the water that will create a plume gets its primary physical properties like salinity. *Marsaleix et al. [1998]* and *Fong and Geyer [2001]*, for instance, set this salinity to zero. In other cases [e.g., *Fong and Geyer, 2002*], it is set to a known value. There are also authors who include in their

model configuration an idealized estuary which can have the form of a buffering tank [*Oey and Mellor, 1993*]. None of those solutions is suitable for our study as the scale of estuaries is too small to be taken into account in ocean GCMs. We want to ignore their internal dynamics but we want to estimate their contribution to the system from a mixing perspective. This has to be done with the only data that we are supposed to know from GCMs: the river pure freshwater flow (and its seasonal variability) and some basic geometrical data on the river mouth (width or hydraulic radius).

[13] In order to solve the problem with accessible global data, we have chosen to consider each estuary as a mixing black box that sends a tide averaged flow of low-density water. To find the salinity for the river inflow on a general case, it is considered that salt water is brought inside the estuary by the baroclinic countercurrent that enters the estuary, as described by *Yankovsky [2000]* and the well-known Figure 1. As one moves up the estuary, the ocean's influence decreases and so does the baroclinic current entering the estuary.

[14] In equation (1), fluxes F_{Sout} and F_{Sin} are defined respectively as salt flux density leaving the estuary and salt flux density entering the estuary. u_{river} is the depth related velocity at the boundary between the estuary and the coastal ocean, and σ is the relative depth as shown on Figure 1.

$$F_{Sin} = \int_{-1}^{\sigma_{int}} u_{river} S d\sigma \quad F_{Sout} = \int_{\sigma_{int}}^0 u_{river} S_{est} d\sigma \quad (1)$$

[15] In order to estimate the salinity of mixed water that leaves the estuary through salt flux F_{Sout} (see Figure 1), the simplest way would be to consider that $F_{Sout} + F_{Sin} = 0$. The estuary, however, has an inertia from a haline perspective, which means it can respond to changes in salt flux (exiting or entering the estuary) with a lag as shown, for instance, by *Monismith et al. [2002]*.

[16] In order to take this aspect into account, we will suppose that mixing within the estuary occurs in a given volume which is defined by equation (2).

$$V = l_m HB \quad (2)$$

l_m stands for a horizontal mixing length that will be defined later, B is the river width and H is defined as the river's depth at its mouth.

[17] The salt flux provided by the river to the estuary is supposed to be nil (i.e., pure freshwater contains no salt). Therefore, if volume V has a given salinity, conservation of salt in volume V yields equation (3).

$$l_m \frac{\partial S_{est}}{\partial t} = F_{Sin} + F_{Sou} \quad (3)$$

[18] Following observations made by *Monismith et al.* [2002] or *MacCready* [1999], if the freshwater flow becomes important, salt penetration is reduced and horizontal salt gradient is compressed toward the mouth of the estuary, which corresponds to a low inertia estuary, hence a low l_m . Conversely, a low river flow will permit a strong penetration of salt in the estuary, which yields an increase of the salt penetration, which corresponds to a strong inertia estuary, hence a higher l_m . Penetration of salt in the estuary is the result of different processes as shown by *MacCready* [2004], who defines four length scales to describe the penetration of salt inside the estuary. As a first approximation, we will suppose that the main process that brings salt up the estuary is driven by tides. Considering only this process as being the main cause of mixing within the estuary supposes that the estuary is partially or well mixed [*MacCready*, 2004]. However, mixing brought by tides will be taken into account in the coastal ocean model using horizontal and vertical diffusion as we will see in subsection 2.2. Therefore, if a boundary condition between the black box estuary and the coastal ocean ensures continuity, then development of the baroclinic currents bringing salt inside the estuary will take this physical aspect into account. Though an important goal to achieve, the complete study of the effects of estuarine parametrization goes beyond the scope of this paper.

[19] If a tidal horizontal diffusion coefficient K_h at the mouth of the estuary is known, then it can be written that $K_h \equiv l_m \bar{U}_{river}$, \bar{U}_{river} standing for river barotropic flow velocity. On the basis of a simple concept of volume and salt conservation, *MacCready* [2004] defined a way to compute tidal diffusion coefficient close to the river mouth (equation (4)).

$$K_h = L_T^2 \frac{1 - \sqrt{\frac{2}{\pi} \frac{B}{L_T}}}{T_T} \quad L_T = \frac{\bar{U}_{est} T_T}{2} \quad (4)$$

[20] In equation (4), L_T is the tidal excursion, B is the width of the river mouth and T_T is the tidal period.

[21] \bar{U}_{est} is taken as the mean estuarine tidal velocity in the estuary during a tidal period, quadratic averaging being used of course. \bar{U}_{est} , L_T are unknown. We will show in subsection 2.2, however, that we can compute them from tidal harmonics for a given tidal period T_T .

2.2. Tidal Mixing

[22] Tidal currents will be taken into account only from an energetic point of view for reasons explained in subsection 1.2. They will be considered as a constant production of turbulent kinetic energy as does *Mellor* [2002] for higher-frequency waves. Equation (5) is the equation of conservation of turbulent kinetic energy q by *Mellor and Yamada* [1982] used in the POM configuration that will be detailed later on. The P_S term stands for shear stress production, and the last right hand side term stands for dissipation of turbulence.

$$\frac{\partial q^2}{\partial t} = \frac{\partial}{\partial z} \left(S_{qt} \frac{\partial q^2}{\partial z} \right) + 2P_S - 2 \frac{q^3}{B_1 l} \quad (5)$$

[23] As dissipation is only related to the turbulent kinetic energy q and to the vertical mixing length l , it is possible to include an extra virtual production of turbulence as proposed by *Mellor* [2002]:

$$P_S = K_M \left[\left(\frac{\partial u}{\partial z} \right)^2 + \left(\frac{\partial v}{\partial z} \right)^2 \right] + P_{Tidal} \quad (6)$$

[24] In which K_M stands for turbulent vertical diffusion coefficient in $m^2 s^{-1}$ and P_{Tidal} stands for the production brought into the system by virtual tidal current.

[25] The field of production of turbulent kinetic energy needs to be established both from a vertical and horizontal point of view.

2.2.1. Vertical Scale

[26] From a vertical point of view first: *Rippeth et al.* [2002] have shown for a channel that tidal current production of turbulent kinetic energy fits a typical steady state law of the wall log function at any given phase of the tide (i.e., vertical diffusion of turbulence is a quick process compared to tidal propagation in shallow regions). For any given point equation (7) is used for vertical distribution of turbulence production [*Rippeth et al.*, 2002]:

$$P_{Tidal} = - \frac{\rho u_*^3}{k} \frac{z}{h(z+h)} \quad (7)$$

u_* standing for tidal friction velocity, k for Von Karman's constant, z for depth and h for bathymetry. In order to estimate u_* , bottom friction can be written as $\tau_b = \rho u_*^2 = \rho C_d U^2$, C_d is the local bottom drag coefficient, and U is the barotropic tidal velocity. This production will be averaged on each T centered vertical grid cell of POM and then interpolated on production point (Q point) in order to take into account grid stretching. Most of the production is located near the bottom, a region where a coarse resolution is chosen (river plume being located near the surface) for computational performance. For a satisfactory treatment of the lower boundary condition, the production is computed over the cell at the T point and then interpolated to the Q points.

2.2.2. Horizontal Scale

[27] Determining u_* requires the horizontal distribution of tidal currents within the area. Tidal wave amplitude and phase have been provided by the Service Hydrographique et

Océanographique de la Marine (SHOM) (French Navy). Tidal currents may be deduced using the method proposed by *Battisti and Clarke* [1982] or *Lentz et al.* [2001] based on the Laplace tidal equations shown in equation (8):

$$\begin{aligned} u_t - fv &= -g\eta_x - \frac{\tau_b^x}{\rho h} \\ v_t + fu &= -g\eta_y - \frac{\tau_b^y}{\rho h} \end{aligned} \quad (8)$$

[28] Equations in which u and v stand for x and y velocities, η for water elevation, t for time, f for Coriolis parameter, τ_b^x and τ_b^y for x and y bottom friction, ρ for water density, h for bathymetry and g for gravity acceleration. Periodic time variation of angular velocity ω is supposed as well as a linear drag coefficient r . Bottom stress components may be expressed as in equation (9):

$$\tau_b^x = \rho r u \quad \tau_b^y = \rho r v \quad (9)$$

[29] Using $i^2 = -1$, equation (8) may be written as equation (10).

$$\begin{aligned} \left(-i\omega + \frac{r}{h}\right)u - fv &= -g\eta_x \\ \left(-i\omega + \frac{r}{h}\right)v + fu &= -g\eta_y \end{aligned} \quad (10)$$

from which u and v can be deduced, as shown in equation (11) using the same approach as by *Cook* [2000]. r is estimated using an iterative method that supposes that $r = C_d|U|$ in which C_d is the bottom drag coefficient computed from bathymetry and bottom roughness using the Chezy formula, and $|U| = \sqrt{u^2 + v^2}$. The bottom roughness z_o is taken equal to 0.01 meters and the Chezy formula is $C_d = g/C_h^2$, with C_h being the Chezy coefficient. The Chezy coefficient can be related to z_o and h by many empirical formulas including the one used by *Ramette* [1981]: $C_h = 26.4(h/z_o)^{1/8}$. Results found are close to *Battisti and Clarke* [1982], who take $r = 5 \cdot 10^{-4} \text{ m s}^{-1}$.

$$\begin{aligned} u &= -\frac{g}{\left(i\omega + \frac{r}{h}\right)^2 + f^2} \left[\eta_x \left(i\omega + \frac{r}{h}\right) + f\eta_y \right] \\ v &= -\frac{g}{\left(i\omega + \frac{r}{h}\right)^2 + f^2} \left[\eta_y \left(i\omega + \frac{r}{h}\right) - f\eta_x \right] \end{aligned} \quad (11)$$

[30] These tidal currents cannot be taken into account for computation of estuarine tidal velocities: their cross shore component will tend to zero while approaching the coast, whereas estuarine tidal velocities are actually mostly cross shore components created by the special geometry of the river mouth. Therefore, for the special case of estuarine tidal velocity, required in the computation of tidal excursion (described in subsection 2.1), the estuary is considered as a simple constant depth channel and in which rotational effects can be neglected. This yields a simplified version of equation (11) for estuarine tidal velocity:

$$u_{est} = \frac{g}{\left(i\omega + \frac{r}{H}\right)} ik\eta \quad \text{with } k = \frac{\omega}{\sqrt{gH}} \quad (12)$$

[31] This estuarine barotropic velocity will be used for computation of estuarine tidal velocity introduced in sub-

section 2.2, and will permit computation of the K_h horizontal diffusion coefficient for each river mouth. For continuity purposes, at the vicinity of each mouth, an additional K_h horizontal diffusion coefficient will be added. It will permit a better simulation of horizontal tidal diffusion near each river mouth. This additional coefficient decreases along a sinus curve to become nil when a distance bigger than the tidal excursion is reached.

2.3. Data Accessibility

[32] The data required to implement the parametrizations described previously is accessible at the global scale.

[33] 1. River flow is accessible from land surface models like the one used by *Ngo-Duc et al.* [2005]. Basic Hydraulic scales may also be deduced to estimate estuarine size. River water temperature and sediment transport may affect water density through many processes. These aspects are not taken into account in land surface models. As most authors do, we consider that density gradients between river water and seawater caused by temperature differences are an order of magnitude bellow density gradients caused by salinity differences.

[34] 2. Tidal harmonics can be provided for any place in the world by various institutions. Bathymetry as well.

[35] 3. Weather reanalysis can be used as a source of forcing as for an ocean GCM when it is not coupled to an Atmospheric GCM. In the case presented hereafter, wind stress data is based on 10 m wind velocities from the ECMWF ERA-40 reanalysis.

3. Model Configuration

[36] A configuration of the Princeton Ocean Model (POM) [*Blumberg and Mellor*, 1987] is applied to the coastal area in the vicinity of the Mekong Delta (Vietnam) shown on Figure 2. Seven branches of the Mekong River and their corresponding mouths (see Figure 2 for names) are taken into account in the configuration. Temperature effects will not be considered in this simulation. The entire coastal ocean configuration and the freshwater flow are set at a constant and uniform temperature. Just like *Hetland* [2005] does, we will consider that the base of the river plume is always high above the thermocline.

3.1. Gridding and Domain

[37] A 300 km \times 300 km square configuration is defined with lower left corner at position 8°N and 105°E. The grid resolution is defined as constant along zonal and meridional axis and taken equal to 2 km. This length is far below the baroclinic Rossby radius of the flow and is an appropriate scale for the width for any of the branches of the Mekong River when it reaches the sea. Vertical resolution of sigma levels consists of 21 points distributed along axis according to a log function which gives high definition close to the surface and lower one close to the bottom. The 2-minute Gridded Global Relief Data ETOP02 bathymetry is used (U.S. Department of Commerce, National Oceanic and Atmospheric Administration, National Geophysical Data Center, 2001). It has been interpolated to the configuration grid, and its shallowest depth is set at 5 m. This depth will be taken as a final depth for the rivers as well.

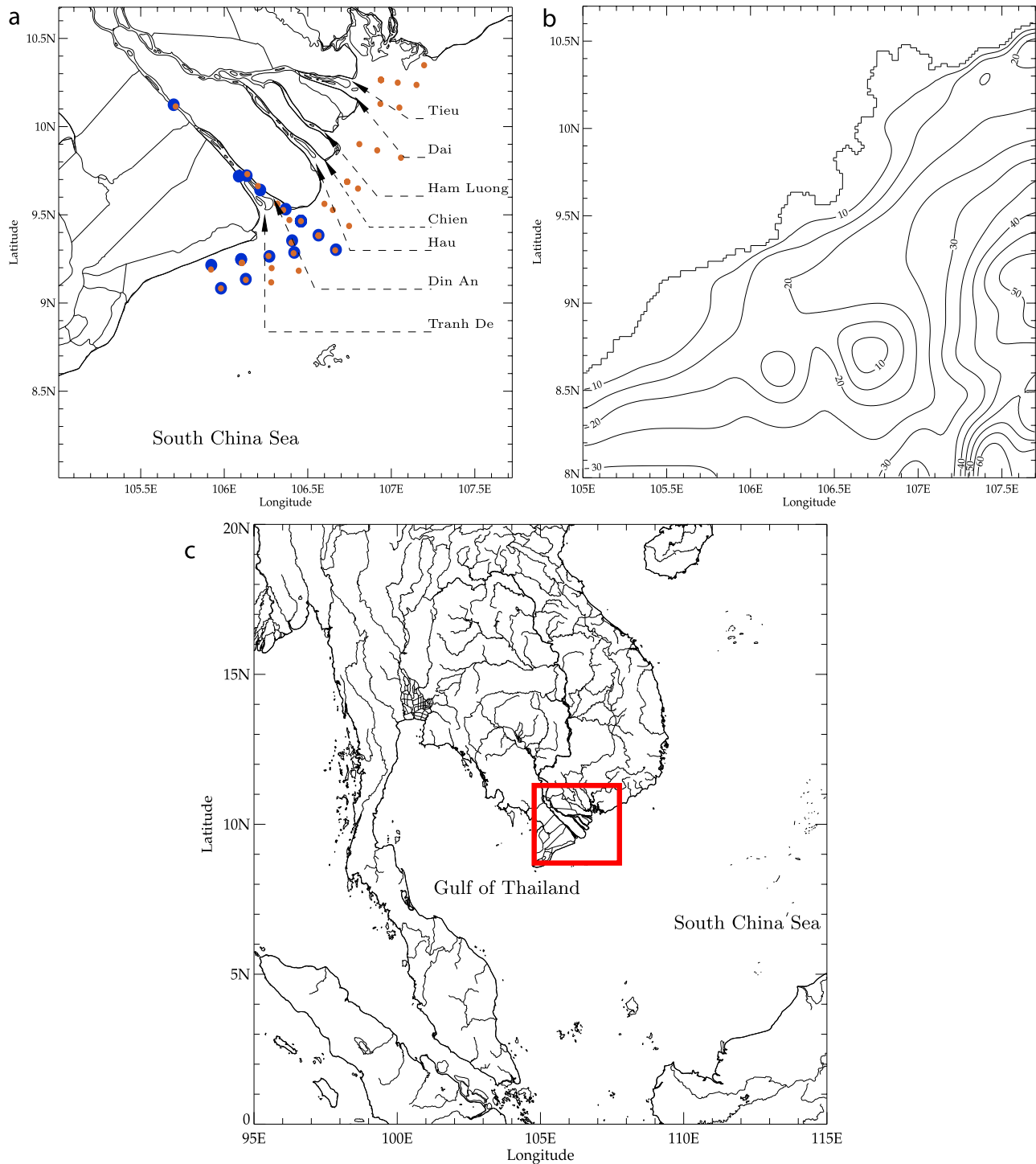


Figure 2. (a) Mekong Delta coastal zone with branches and (b) configuration's bathymetry (in meters) and coastline. Dots on Figure 2a show the position of CTD measurements made during the Cuu-Long campaign in 1997 [Hungspreugs, 1998], blue dots are for the campaign carried out in March 1997, and red dots are for the campaign carried out in October 1997. (c) Geographical position of the Mekong delta on the South Eastern Asian shelf.

3.2. Boundary Conditions

3.2.1. Open Boundaries

[38] At the open boundaries of the domain, *Flather* [1976] radiation for barotropic flows is applied whereas internal mode flows have a zero derivative boundary

condition applied. Apart from tidal currents, the large-scale currents in this area are mostly wind driven as can show some outputs of the OPA Ocean GCM [Madec *et al.*, 1998]. As wind is taken into account in the present simulation, we have not considered any forcing currents at the boundaries

Table 1. Known or Estimated Data for Each Mouth of the Mekong Delta

Mouth Name	Mean Est. Tidal Vel., ^a m s ⁻¹	K_h Diff. Coeff., ^a m ² s ⁻¹	Dry Season ^b	Wet Season ^b
Tieu	0.20	653	6%	11.3%
Dai	0.23	788	16%	12.6%
Ham Luong	0.24	811	13%	12%
Chien	0.23	724	15%	12.5%
Hau	0.26	972	28%	20.6%
Din An	0.33	1661	28%	20.6%
Tranh De	0.34	1843	21%	23.3%

^aMean tidal velocities for each river mouth of the Mekong Delta, with corresponding horizontal diffusion coefficients computed according to *MacCready* [2004]. Mouth order goes from north down south. For a given barotropic river flow of 0.1 m s⁻¹, l_{mix} values range from about 6 km up to 18 km.

^bDistribution of total freshwater flow in the Mekong Delta branches during dry and wet seasons [from *Hungspreugs*, 1998].

of the configuration. Salinity boundary conditions are taken as continuous for exiting streams but entering ones are set with time-moving salinities based on *Levitus et al.*, 1994].

3.2.2. River Boundaries

[39] At the outputs of the delta branches, a zero derivative for η is set, salinity of the exiting water is computed using equation (3) with l_m being computed from the K_h estuarine horizontal diffusion coefficient. K_h is derived from \bar{U}_{est} estuarine mean tidal velocity and using equation (4). Results are shown in Table 1 for each branch of the Mekong Delta.

[40] The total upstream freshwater flow is taken from the climatology shown on Figure 3 for each month of the year and its distribution in each branch are given by *Hungspreugs* [1998]. It is reproduced on Table 1. Imposed freshwater flow in each branch yields exiting barotropic flow from the estuary U_{river} . Once this data is known, the boundary condition given by *Yankovsky* [2000] is used (reproduced in equation (13)) to find internal mode velocities u_{river} for each sigma level.

$$u_{river}(\mathbf{x}, \sigma) = u(\mathbf{x} + \Delta\mathbf{x}, \sigma) \frac{U_{river}}{\int_{-1}^0 u(\mathbf{x} + \Delta\mathbf{x}, \sigma) d\sigma} \quad (13)$$

\mathbf{x} standing for the position of velocities at the output of the black box estuary, and $\mathbf{x} + \Delta\mathbf{x}$ for the position of velocities at the neighboring grid point in the cross-shore direction. This boundary condition gives an estimate of the flow entering and exiting the estuary, which permits to establish F_{Sin} and F_{Sout} fluxes required for salt balance computation of equation (3). F_{Sin} will be computed using u_{river} and for a salinity which is known for each σ level at position $\mathbf{x} + \Delta\mathbf{x}$. F_{Sout} will be computed using u_{river} and S_{est} estuarine mixing salinity described in equation (3). In the meantime, *Yankovsky* [2000] has shown this boundary condition to be much closer to the problem's physics and limits upstream intrusion of freshwater found by many authors.

3.3. Tidal Production of Turbulence

[41] The extra source of vertical mixing presented in subsection 2.2 has been computed on the most energetic tidal component which happens to be the $K1$ wave in this region. The results are shown in Figure 4 for the mean $K1$ tidal velocity. One can notice that tidal velocity decreases when approaching the coast as its cross-shore component becomes small.

3.4. Extra Settings

3.4.1. Numerical Settings

[42] From a numerical point of view, *Smolarkiewicz* [1984] advection scheme is used; *Smagorinsky* [1963] diffusion coefficient is set to 0.1, the external time step is set to 20 s while the internal time step is set to 600 s except during Mekong's flood season at the end of summer where it is lowered to 400 s because of offshore extension of the plume that develops fast internal waves in deep regions.

3.4.2. Experimental Settings

[43] The experiment starts on 1 January 1997 and the initial state is constant salinity in the computational area with zero velocities. Experience has shown that the baroclinic current created by the input of low-density water reaches the westward boundary of the domain before the end of January, but first results shown are for the month of March, so the spin up time is about two months.

4. Results: The Mekong River Plume in 1997

[44] Results presented hereafter focus on the two months of year 1997 for which CTD measurements have been made off the coast of the Mekong Delta as part of the Cuu-Long

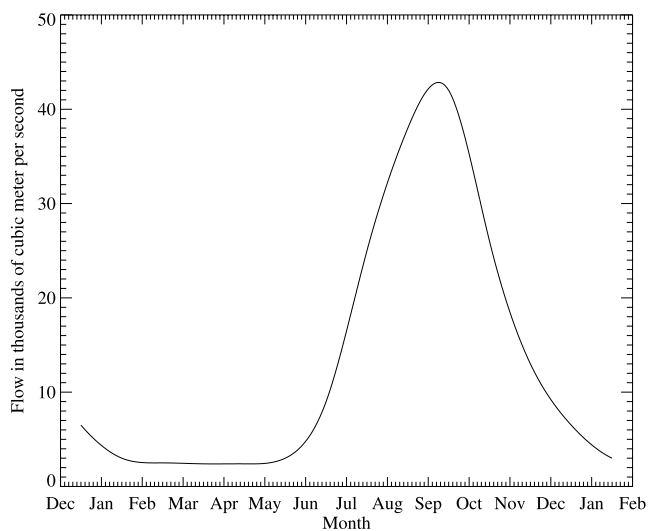


Figure 3. Mekong freshwater flow in thousands of m³ s⁻¹, averaged over 27 years in the period 1933–1966 [from *Simpson and Snidvongs*, 1998].

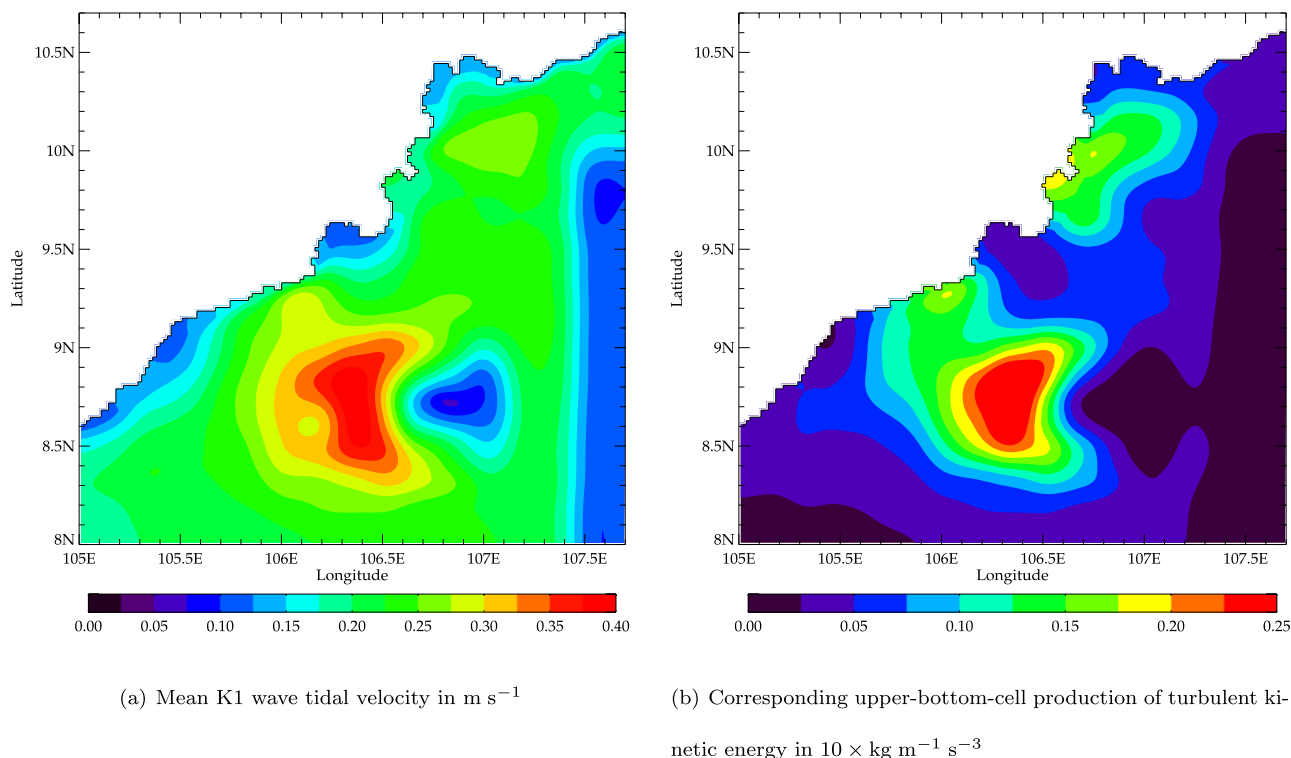


Figure 4. (a) K1 wave mean tidal velocities in the Mekong Delta coastal zone and (b) corresponding production of turbulent kinetic energy near the bottom. Computed from tidal height and phase provided by the SHOM, Service Hydrographique et Océanographique de la Marine.

project [Hungspreugs, 1998; Landmann et al., 1998]. Measurements were made in March and October 1997.

4.1. A Dry Season Case: Month of March

[45] During the dry season, the Mekong total flow is about $2500 \text{ m}^3 \text{ s}^{-1}$. Wind blows from N-E and will tend to create an Ekman transport toward the coast (downwelling case) and compress the plume against it. This is consistent for instance with the study made by Garcia Berdeal et al. [2002], who find similar results in the case of the Columbia river when the wind blows from the south. However, wind stress at water surface stays at quite a low average mean value of about 0.03 N m^{-2} as shown in Figure 5. A baroclinic current is created by the input of low-density water and heads SW leaving the coast on its right and as shown on Figure 5. The flow is mainly created by the four lower mouths of the Mekong Delta (Dinh An, Tranh De, Hau and Chieu) that provide a consistent flow of low-density water to the coastal area. Vertical mixing plays a major role. The upper mouths (Dai, Ham Luong) provide less water but the weakness of the baroclinic current is also explained by the shallow bottom extending far offshore there. Figure 6 shows an offshore extension of freshwater influence but very low stratification on the shallow region, yielding a very weak current. Downshelf of the lower mouths, the current encounters a shallow bottom again and its stratification is destroyed by vertical mixing as shown on Figure 7. The main current stays off the shallow area located down the lower mouths of the Mekong Delta. The current then sticks to the coast and is likely to end its course in the Gulf of Thailand for which it provides an

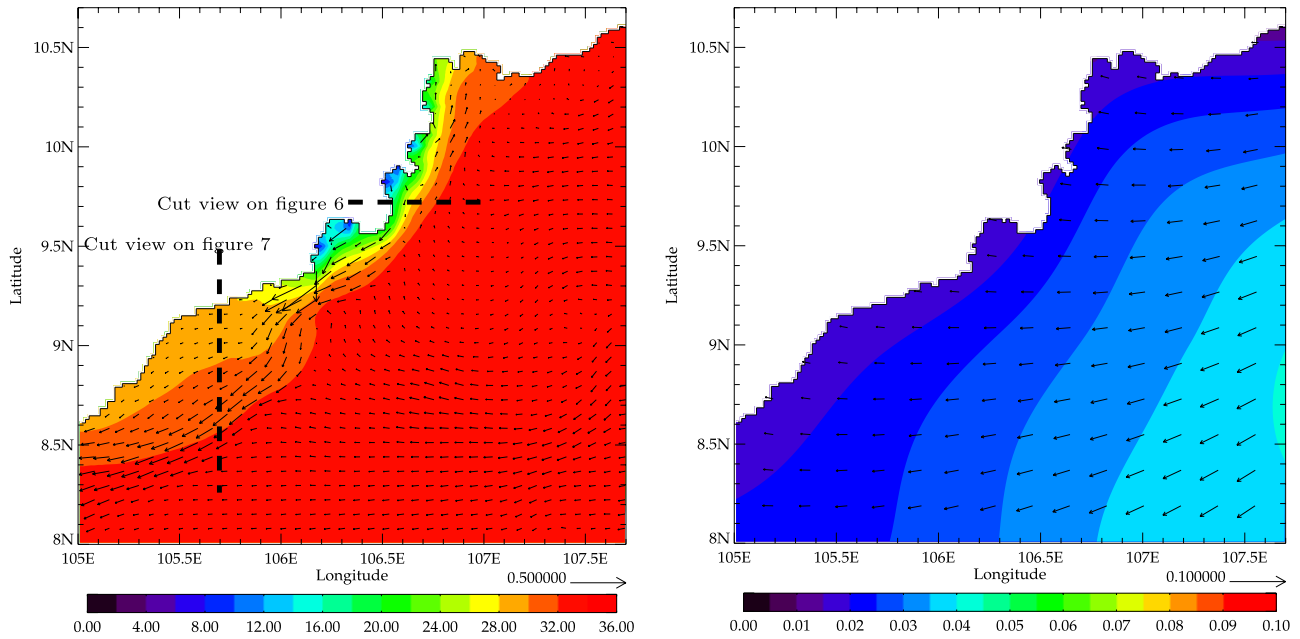
important source of stratification as mentioned by Simpson and Snidvongs [1998]. From a more general perspective, there is a strong interaction between the bottom and the river plume and we can notice the formation of areas of low-density water with low dynamics. The plume is bottom advected and the strongest source of tidal mixing being located close to the bottom enhances this aspect. An important amount of the potential vorticity brought by the freshwater inflow is absorbed by the tidal mixing, which reduces the dynamics generated by the river plume in the coastal area.

4.2. A Wet Season Case: Month of October

[46] The Monsoon ends up in October. The Mekong freshwater flow reaches a value of $35000 \text{ m}^3 \text{ s}^{-1}$. The peak value of about $40000 \text{ m}^3 \text{ s}^{-1}$ is close to the mean flow of the Congo River [Dai and Trenberth, 2002] and occurs in September. Wind forcing has radically changed during the summer months from a NE dominant wind in march to a SW dominant wind. Wind still blows from SW at the beginning of October but reverses at the end of the month to become N-E dominant again as the Monsoon winds end.

4.2.1. First Days of October

[47] During the first five days of the month, wind blows from SW (upwelling type). It strongly advects freshwater high flow offshore as shown on Figure 8. Wind forcing is very homogenous over the domain both in strength and in direction but surface velocities differ widely depending on their location. Outside the river plume area, velocities of small amplitude almost follow wind stress direction. This situation is entirely different for the low-salinity area in



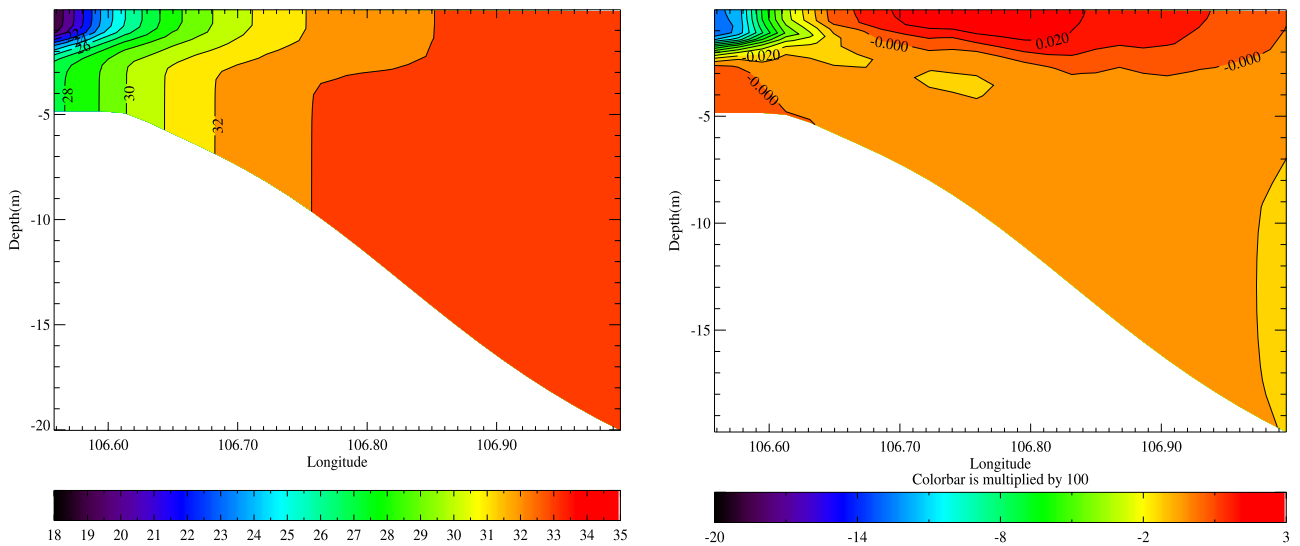
(a) Mean surface salinity (psu) and current ($m s^{-1}$)

(b) Mean Wind stress direction and norm ($N m^{-2}$)

Figure 5. (a) Monthly mean for March 1997 for surface salinity and surface current and (b) wind stress. Wind stress data have been computed using *Garratt [1977]* and 10 m wind velocities from the ECMWF ERA-40 reanalysis.

which strong velocities may be observed with direction heading toward SE. This can be explained by the higher stratification in the river plume which will affect freshwater plume. The important stratification at the bottom end of the plume will block vertical diffusion of turbulent kinetic energy and concentrate momentum transmitted through

wind stress on the thin vertical scale of the plume, this will be especially true once the plume is far enough off the coast where stratification can not be destroyed by the bottom friction induced by motion and tidal mixing. This acceleration of river plumes is also described by many authors and particularly clearly by *Fong and Geyer [2001]* in a similar



(a) Mean salinity (psu)

(b) Mean velocity ($m s^{-1}$)

Figure 6. Zonal cut for (a) salinity and (b) meridional velocity at $9.7^{\circ}N$ and between $106.55^{\circ}E$ and $107^{\circ}N$ (see Figure 5) and monthly mean for March 1997. For a better description of the haline stratification the scale has been changed from Figure 5.

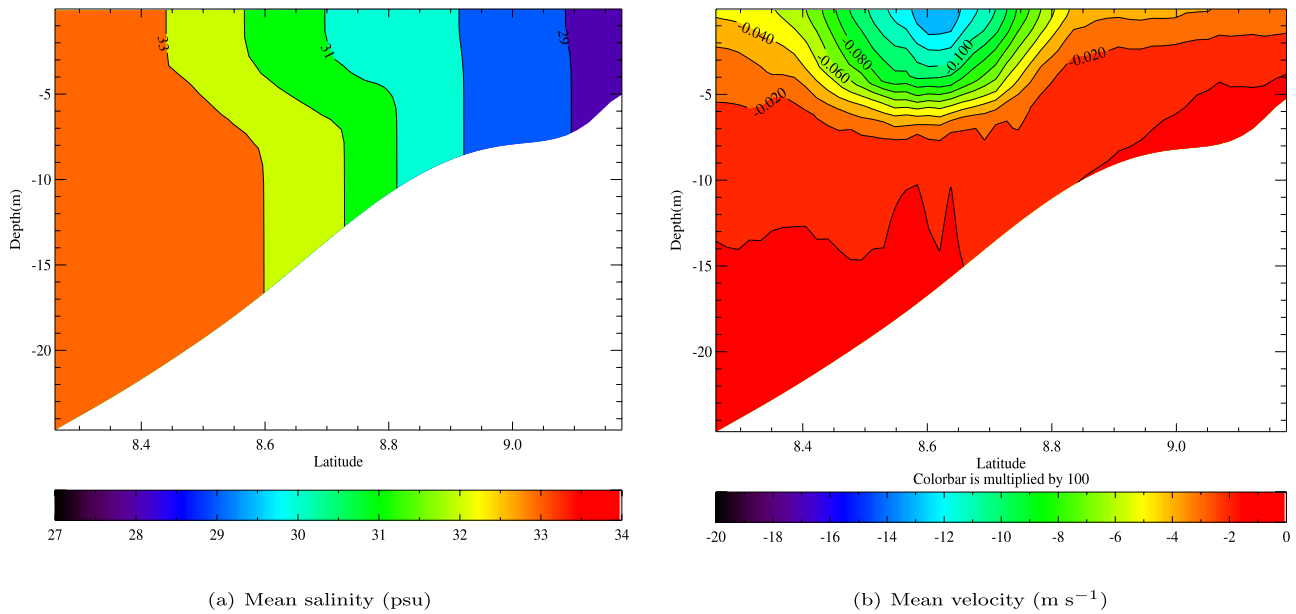


Figure 7. Meridional cut for (a) salinity and (b) zonal velocity at 105.7°E and between 8.3°N and 9.2°N (see Figure 5) and monthly mean for March 1997. For a better description of the haline stratification, the scale has been changed from Figure 5.

upwelling case. Figure 9 shows a strong link between density stratification and high zonal velocities.

4.2.2. End of the Month of October

[48] At the end of October, winds have reversed and a weak NE wind blows again within the Mekong Delta area. River flow decreases but is still at a very high level compared to the dry season. Result is a broad plume

sticking to the coast and flowing again with the coast on its right. Many differences, however, can be observed with the month of March. The plume is wider (see Figure 10) and its stratification is higher as shown on Figure 11. Thanks to the bigger inflow of freshwater in the coastal area, a bigger baroclinic current is created with velocities twice as large as the ones observed in March. Salinities range from very low

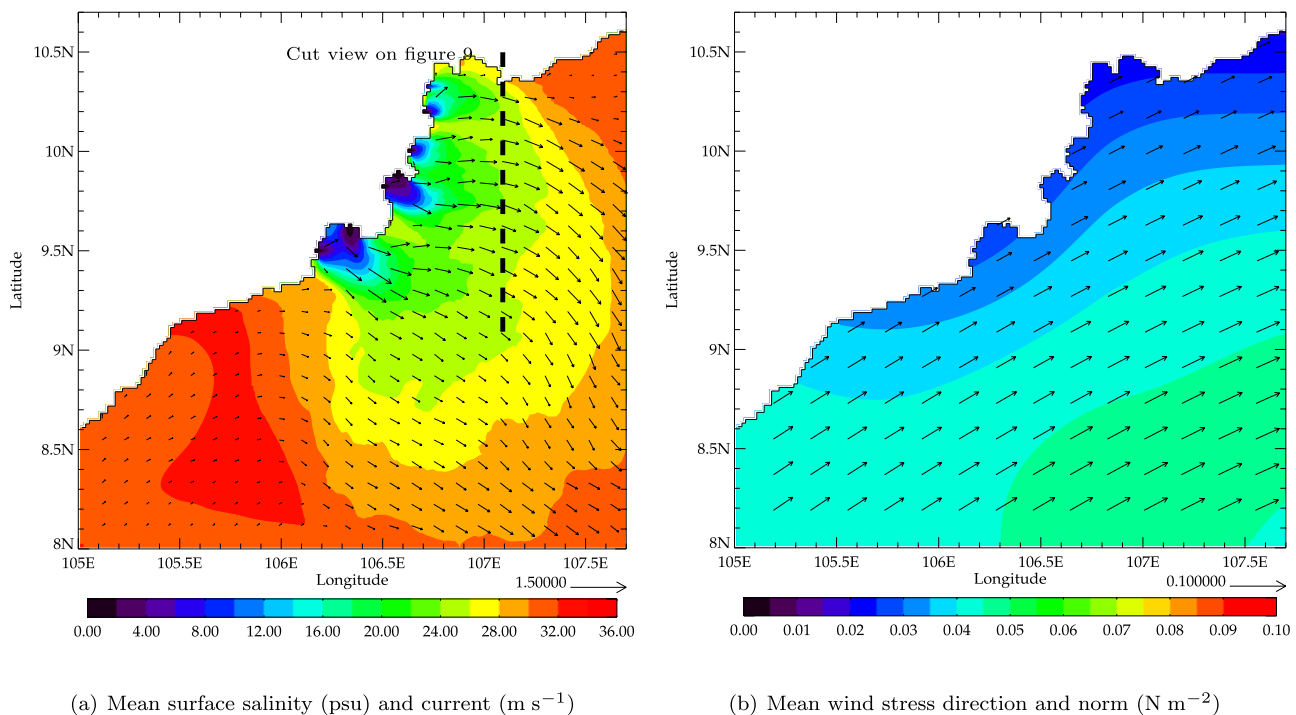


Figure 8. (a) Surface salinity and surface current and (b) wind stress, averaged between 1 and 5 October 1997.

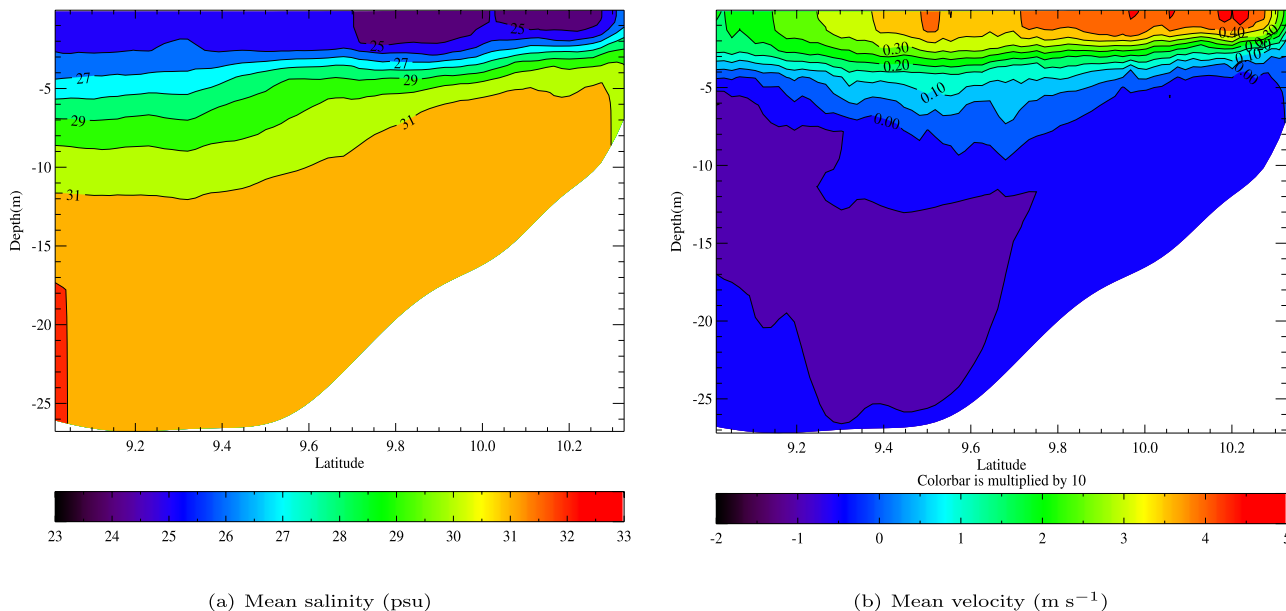


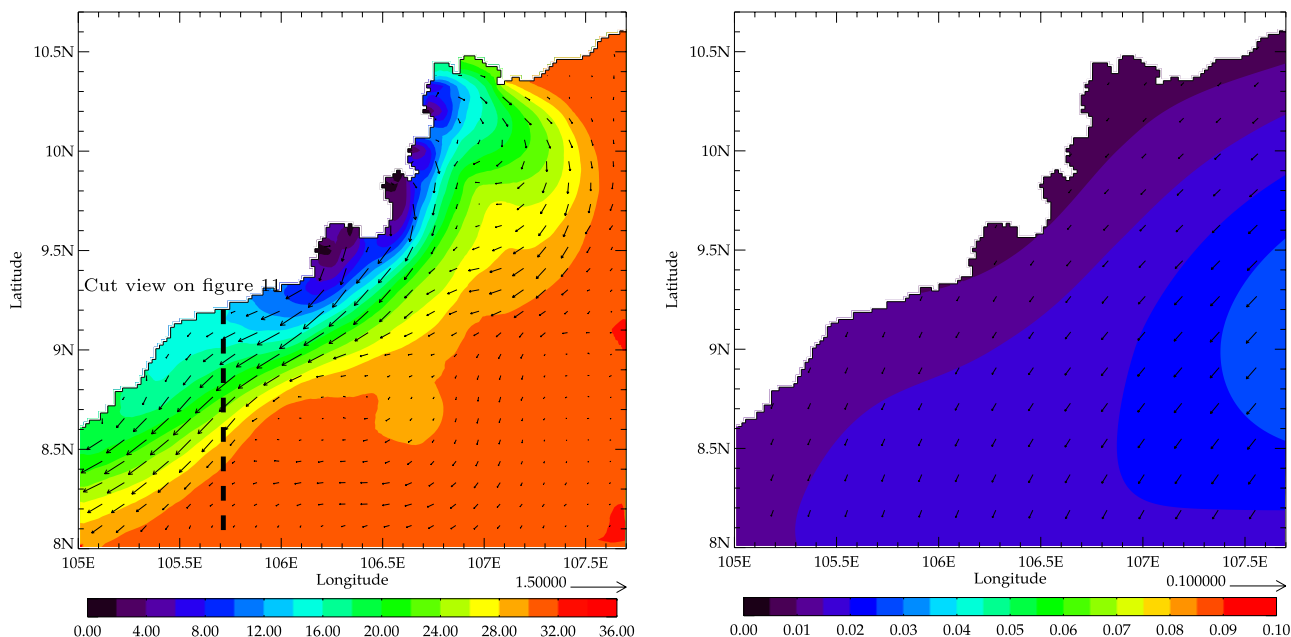
Figure 9. Meridional cut for (a) salinity and (b) zonal velocity at 107.1°E and between 9°N and 10.5°N (see Figure 8), averaged between 1 and 5 October 1997. For a better description of the haline stratification, the scale has been changed from Figure 8.

values of less than 20 psu at the coast to 32 psu, explaining strong baroclinic pressure gradient. However, velocities remain low close to the coast as vertical mixing creates a non stratified buffer of low-density water. Once further away from the coast, turbulence destroys stratification in the lower layers and leaves strong haloclines free to develop close to surface. Although the plume is still bottom advected, the potential vorticity brought by the freshwater

inflow is less absorbed by the tidal mixing. This can be explained by the larger extent of the plume off the coast where tidal production of turbulence can hardly reach the surface.

4.3. Comparison With Observations

[49] The Cuu-Long campaign on the Mekong Delta was held in March and October 1997 [Hungspreugs, 1998].



(a) Mean surface salinity (psu) and current ($m s^{-1}$) (b) Mean wind stress direction and norm ($N m^{-2}$)

Figure 10. (a) Surface salinity and surface current and (b) wind stress, averaged between 15 and 30 October 1997.

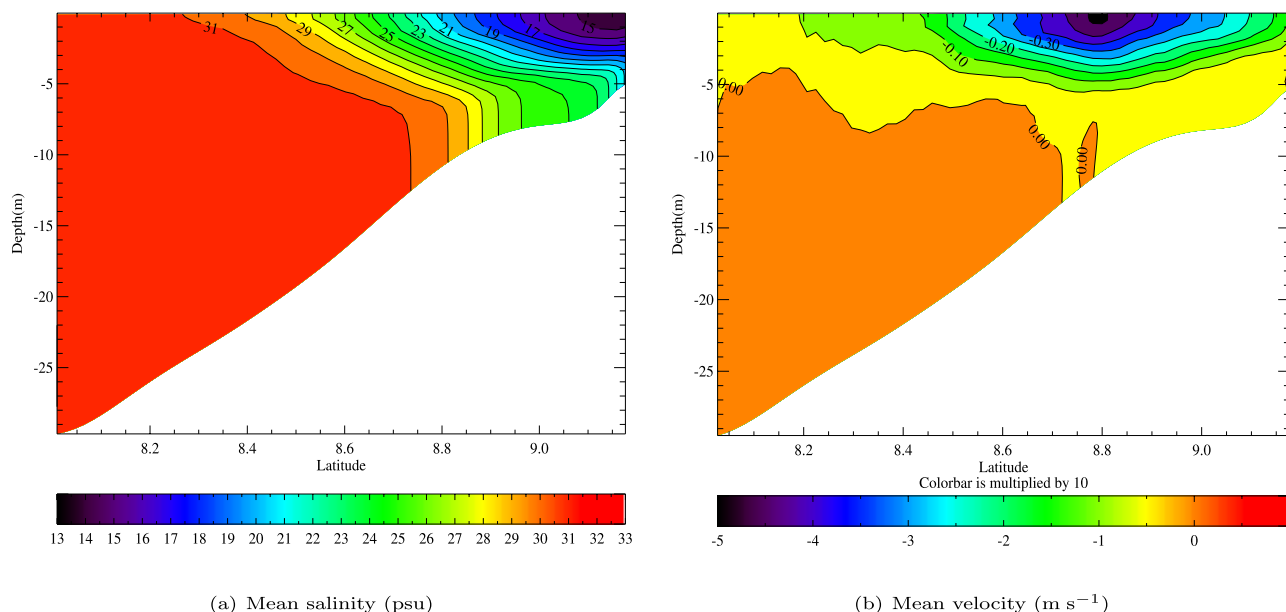


Figure 11. Meridional cut for (a) salinity and (b) zonal velocity at 105.7°E and between 8°N and 9.25°N (see Figure 10), averaged between 15 and 30 October 1997. For a better description of the haline stratification, the scale has been changed from Figure 10.

Cruises were conducted off the coast of Vietnam and CTD measurements were made. Salinity was measured along with other components including pollutants carried from the Vietnamese continental shelf down to the South China Sea. Left-hand side of Figure 2 shows the distribution of all the stations for the two cruises made in March and October 1997.

[50] For each CTD measurement made, model data has been interpolated in space and time. A salinity profile has been computed at location and time of each CTD measurement data. Results are displayed in the chronological order of the observations. About 50% of the measurement stations profiles are shown. Exclusions are made though when the measurement was made inside branches of the Mekong River, and for some stations that are very close to the coast and for which coastline and bathymetry imprecision leads to some unrealistic results of the model.

4.3.1. Campaign in March

[51] Results are shown on Figure 12. Profiles on Figure 12 confirm that the plume does not extent too far off the coast in the model. It shows there is almost no halocline on profiles. Plume behavior is well described by the model as its offshore limit is well reproduced. However, imprecisions on the placement of mouth or on the coastline description lead to some bigger errors when one moves too close to the coast (St.03). The number of CTD measurements in March is small but they show good consistency with the model: the river plume is thin and compressed against the coast. In the observations as well as in the model, there is not sharp halocline which thus explains the weakness of the baroclinic currents along the coast. Most errors can be observed on surface salinity while approaching the plume, but the shape closely describes the plume behavior which is the one of a well-mixed plume from a vertical point of

view. It is probably on measurements made in October that it will be possible to spot the qualities and deficiencies of our configuration, as the number of CTD and their geographical extent is greater.

4.3.2. Campaign in October

[52] CTD measurements made in October were done during the transitional period in which the Mekong River plume evolves from a plume brought offshore by upwelling winds to a coastally trapped plume. First measurements were made on 4 October 1997, and the last one is made on 10 October 1997 which corresponds to the transitional period described in subsection 4.2. Comparison with measurements shows that the behavior of the river plume is well reproduced. From a temporal point of view, the extent of the plume off the coast is confirmed by measurements on Figure 13: the plume extends close to the Northern coast of the area at the beginning of the month of October. Other figures show that the model reproduces well the main features of the river plume, and especially two important points.

[53] 1. The vertical shape of the plume is well described. One can notice on many figures a step on the halocline at a depth of about 5 m which corresponds to the depth of the shallow shelf close to the estuary and in which tidal mixing will have a major influence. Tidal mixing in shallow areas has a conditioning effect on the vertical shape of the plume and its influence can be spotted on the structure of the profile even after low-density water has reached deeper locations.

[54] 2. Although errors may be noted on Figure 14, the surface salinity found by the model is close to reality in most cases. In some cases, we can notice a lack of mixing near the surface that causes the surface salinity to be too low. As mixing near the surface is mostly caused by wind

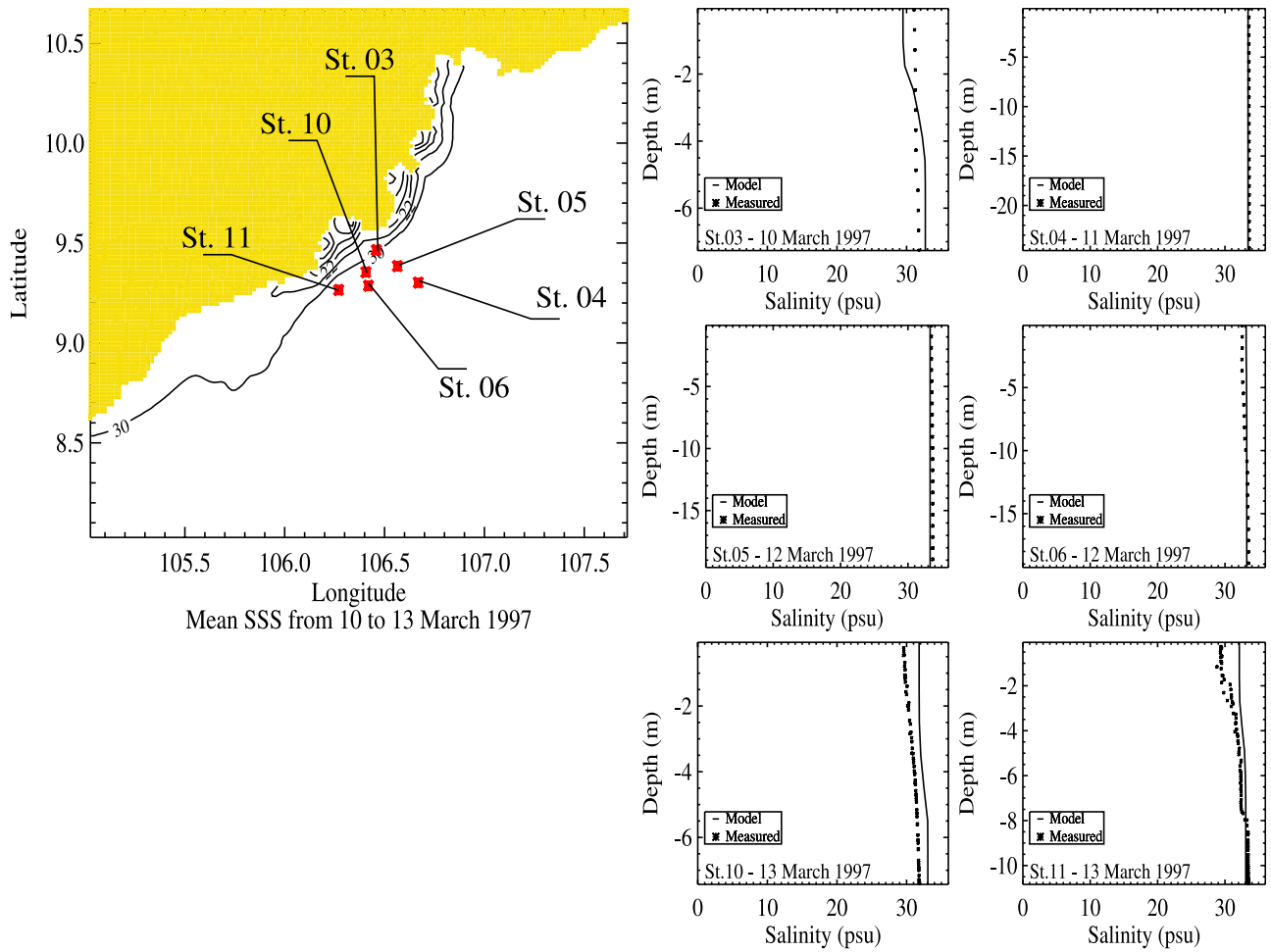


Figure 12. Salinity profiles and corresponding SSS for some measurement stations of the Cuu-Long campaign [Hungspreugs, 1998], month of March 1997.

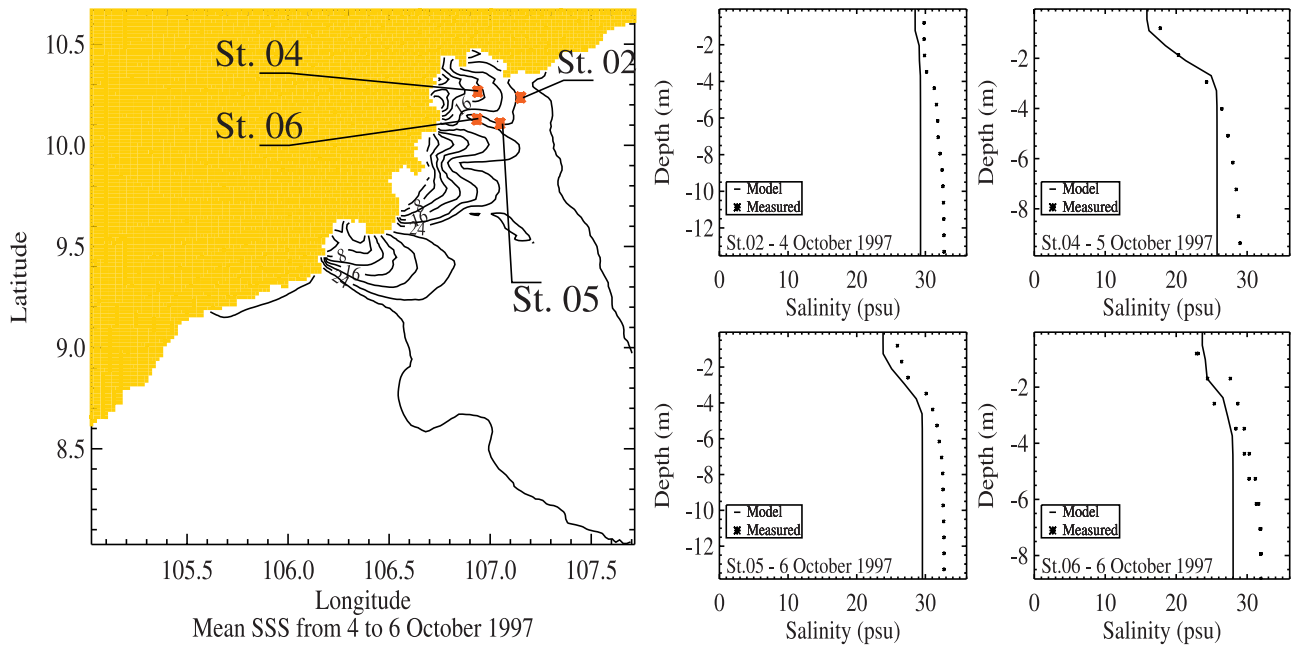


Figure 13. Salinity profiles and corresponding SSS for some measurement stations of the Cuu-Long campaign [Hungspreugs, 1998], 4–6 October 1997.

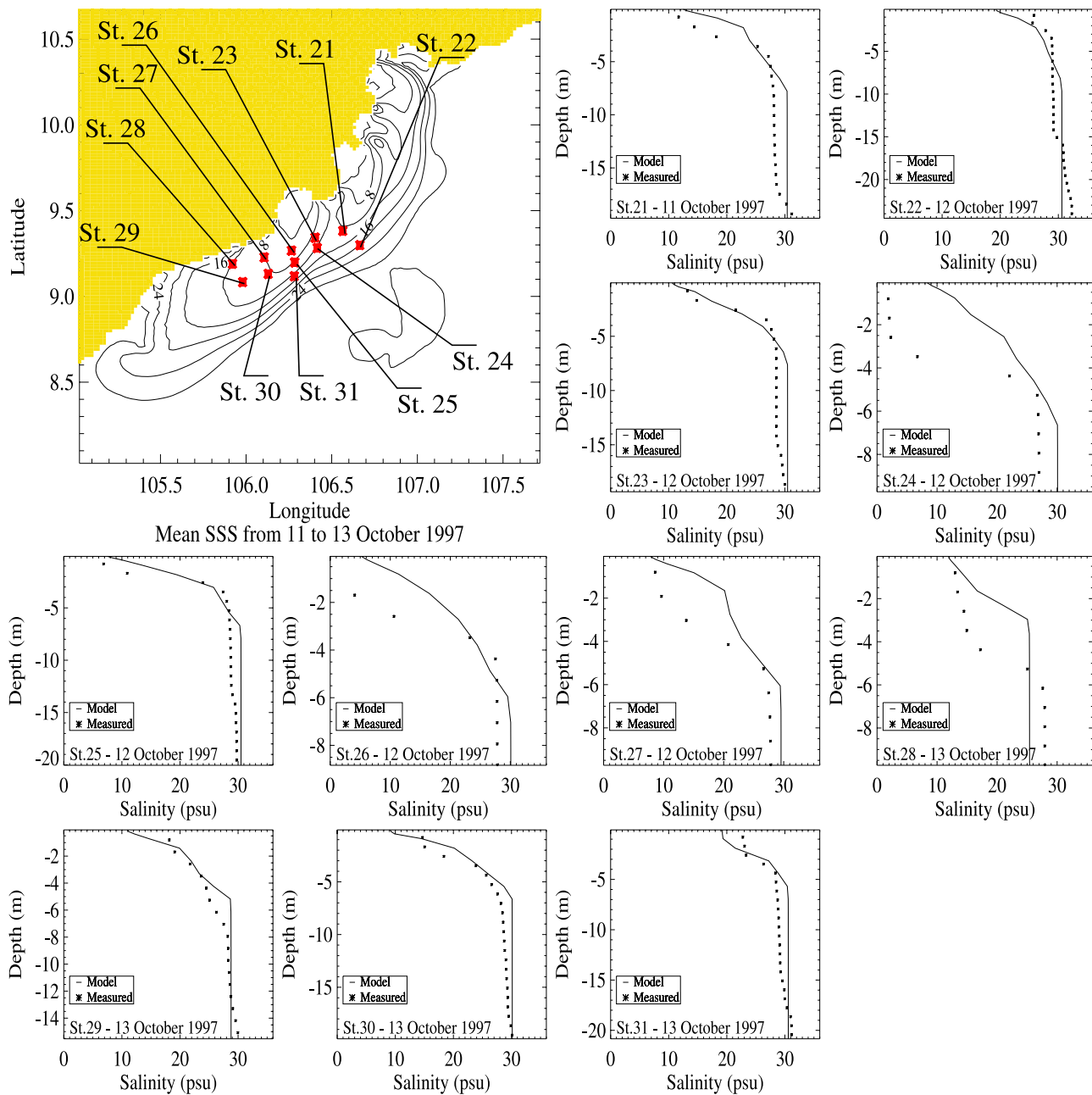


Figure 14. Salinity profiles and corresponding SSS for some measurement stations of the Cuu-Long campaign [Hungspreugs, 1998], 11–13 October 1997.

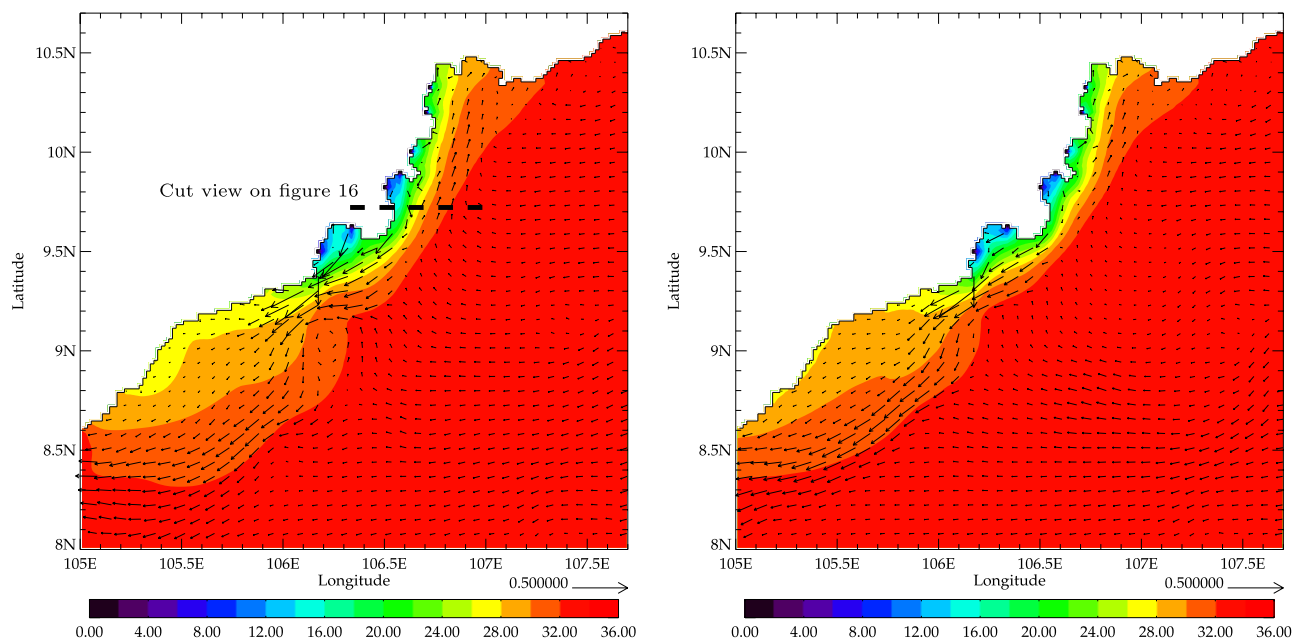
stress, we can conclude SSS errors may be caused by small time imprecisions in the wind forcing.

5. Comparison Between Explicit Tidal Forcing and Tidal Mixing Parametrization

[55] The parametrization of tidal mixing that has been proposed in subsection 2.2 considers only tidal mixing as a time-averaged input of energy in the system that will provide vertical turbulence influencing river plume dynamics. This choice has been made to fit the methods used in Ocean GCMs where tides are considered from the point of view of their average dissipation [Munk and Wunsch, 1998]. In order to validate the parametrization that has been

proposed, we have conducted two extra simulations over the 1997 twelve months period. The previous configuration is used although a few changes are made as described hereafter. The first simulation has been set with an explicit tidal forcing. The K1 tidal harmonic that has been used for the tidal currents computation in subsection 3.3 is also used. Its amplitude and phase are interpolated on the boundaries of the domain and the *Flather* [1976] boundary condition is forced with a variable sea surface height. Of course, all the proposed parameterized sources of vertical tidal mixing are disabled within the computational domain.

[56] The second simulation does not include explicit tidal forcing but only vertical mixing within the computational domain, as already done in section 4. In both simulations,



(a) Mean surface salinity (psu) and current (m s^{-1}), explicit tidal forcing

(b) Mean surface salinity (psu) and current (m s^{-1}), tidal mixing parametrization

Figure 15. Surface salinity and surface current, averaged between 1 and 31 March 1997, comparison between (a) explicit and (b) implicit tidal forcing.

the estuarine mixing parametrization is disabled. The physics of the estuarine parametrization are based on an assumption of a flow for which dynamics are dominated by baroclinicity, and adding an explicit barotropic flow makes it incoherent to use. Therefore the estuarine boundary condition proposed in subsection 2.1 is changed to a simple inflow of pure fresh water as done previously by many authors. The estuarine boundary condition used becomes equivalent to the one used by *Kourafalou et al.* [1996a]. In both simulations, the daily outputs are fields averaged over a tidal period. We have made comparisons for the same months than in section 4.

5.1. Comparison in March

[57] Figure 15 shows the mean surface salinity and currents for the month of March 1997 as simulated by the configuration, once with explicit tidal forcing (left-hand side), the other one with only tidal parametrization (right-hand side). Because of the domain open boundary conditions, we can notice that the extent of the plume downstream is smaller when explicit tidal forcing is used. This is not due to any physical difference of parametrization between the two cases but to the fact that incoming tidal streams advect salt water inside the domain whereas outgoing ones advect water containing salinity anomaly outside the domain. We would not have seen any differences at this place if the domain had been more extended westward.

[58] Although the main shape of the river plume looks very similar, we can notice the following differences between the two cases: (1) there is a low-salinity front close to the coast that is more extended in the downstream area

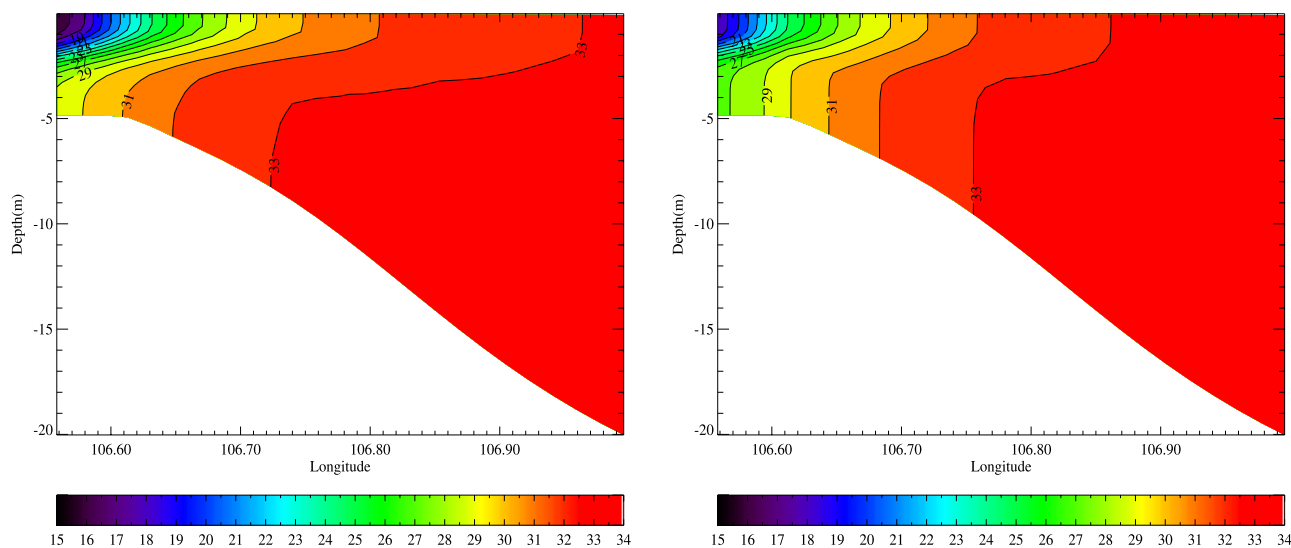
when explicit forcing is used. (2) The surface velocities are slightly stronger when explicit forcing is used. This is specially true close to the southernmost branch of the Mekong Delta. These differences indicate mainly two aspects about the effects of our tidal parametrization.

[59] 1. On the one hand, our tidal mixing parametrization is slightly over estimated in some places. This creates some light differences of stratification as illustrated on Figure 16. These differences of stratification induce baroclinic current velocities which are lower when the tidal mixing parametrization is used.

[60] 2. On the other hand, our tidal mixing parametrization does not take into account horizontal effects created by tidal currents. From an average point of view, tidal currents tend to create a horizontal alongshore diffusion that brings some low-salinity water downshelf in very shallow regions where the lack of stratification does not permit baroclinic currents to be active enough. This explains the greater extension of a freshwater front when an explicit tidal forcing is used as illustrated on Figure 15a). As tidal currents are also more sensitive to bathymetry changes, this kind of resulting horizontal diffusion effect may also explain that density fronts are slightly broader when explicit tidal forcing is used.

5.2. Comparison in October

[61] The differences between explicit tidal forcing and tidal mixing parametrization are even less in October than could be noticed in March. As baroclinic currents are much stronger in October, the horizontal diffusion resulting from the mean effect of tidal currents are even harder to spot. Meanwhile, we have noticed (figures not shown in this



(a) Mean salinity, explicit tidal forcing (psu)

(b) Mean salinity, parametrization of tidal mixing (m s^{-1})**Figure 16.** Zonal cut for salinity at 9.7°N and between 106.55°E and 107°N (See Figure 15).

paper) some small differences of stratification that confirm that our estimation of tidal mixing is slightly over estimated in some regions.

5.3. Validity of Tidal Mixing Parametrization

[62] We have tried to estimate the impact of vertical tidal mixing on the river plume dynamics. In order to achieve this task, we have computed an estimation of the production of turbulent kinetic energy brought by tides over a tidal cycle. From the comparison between explicit tidal forcing and tidal mixing parametrization, it appears that our estimation is sound in most cases. However, we can notice two things.

[63] The first thing is that we only take into account the vertical mixing brought by tides in our parametrization, so we could notice that some horizontal effects are not considered and that there are some small differences from a horizontal perspective. Some fronts are created in very shallow regions by the barotropic nature of the tidal currents when explicit tidal forcing is used, but the freshwater flux in these fronts remains insignificant as the baroclinic velocities in these fronts are themselves negligible. If we focus on the fluxes of salt, freshwater, and momentum entering or exiting the region of freshwater influence, which means on the dynamical features of the region of freshwater influence, this kind of difference can be neglected.

[64] The second thing is that our vertical tidal mixing is slightly over estimated in some regions, and this has an influence on the baroclinic velocities. This can be the result of a number of factors as for instance the way the bottom drag coefficient is estimated in our offline computation of tidal currents and tidal production of turbulent kinetic energy. As the only possible difference in stratification comes from a slightly different estimation of the production of turbulent kinetic energy, this mostly demonstrates one important thing; In tidally dominated coastal regions where tropical rivers often end their continental journey, the river plume dynamics are sensitive to tidal mixing. This confirms

the hypothesis made by *Simpson* [1997] but also what was already noticed by *Geyer* [1995].

6. Discussion and Conclusion

[65] A numerical study of the Mekong River plume was performed using data accessible at the global scale. This restrictive choice has been made to study whether it is possible for global oceanographers to take freshwater runoff from tropical rivers into account in a proper way, and select the parameters that would have to be taken into account in GCMs. To achieve this aim, some important processes that shape the structure of a tropical river plume flowing on a shelf have been listed according to what can be found in the literature. A configuration of the Princeton Ocean Model has been set up and structuring processes for the fate of the tropical river plume have been taken into account, either explicitly (as for wind) or parametrized (estuaries, vertical tidal mixing). Parametrizations rely on data accessible at the global scale: tidal characteristics (for tidal mixing) or simple geometry assumptions (for estuaries). A year-long simulation has been performed for year 1997. Simulation results show behavior which corresponds to what is described in the literature for river plumes. Main differences with mid-latitude river plumes come from the fact the continental shelf off the coast is very shallow, the river mouth being itself located in a sedimental plain. The low Coriolis number also influences the shape but it has been shown that the large amount of fresh water brought by the river still creates a baroclinic coastal current flowing in the direction of propagation of the Kelvin wave. In the case of an upwelling wind, which in this case occurs at time of flood, an offshore directed Ekman transport is shown to exist because of the high stratification induced by the big amount of freshwater brought into the coastal zone.

[66] The classification of freshwater inputs given by *Garvine* [1995] may be used to establish the main features of the Mekong river plume. Table 2 shows the Rossby,

Table 2. Scaling Analysis of the Mekong River Plume for the Months of March 1997 and October 1997

	March (Dry Season)	October (Wet Season)
Kelvin number	1.5	2.46
Froude number	0.55	0.1
Rossby number	0.36	0.22
Rossby radius, km	12	20

Kelvin and Froude Numbers as well as the Rossby radius for the cases that have been studied before. The Kelvin and Froude numbers have been computed just as *Garvine* [1995] did just downshelf of the southernmost estuary where the plume includes all the freshwater inflows of the Mekong delta. In order to avoid wind related effects, the scaling analysis for the month of October 1997 is done at the end of the month. The Coriolis parameter has a fixed value, $f = 2.5 \times 10^{-5} \text{ s}^{-1}$. The Rossby number is taken as equal to the ratio of the Froude and of the Kelvin numbers.

[67] From the scales shown above, we can basically conclude that the Mekong river plume has an intermediate behavior. Its Kelvin number is always above one, but only reaches a high value (according to *Garvine* [1995]) during the wet season. Meanwhile, the low Froude number distinguish it from a simple jet of low-density water and the simulations showed the plume is dominated by geostrophy from a dynamical perspective: its freshwater is advected by a coastally trapped baroclinic current. The Rossby number that always stays below one confirm this aspects. We have seen in numerical simulations that there is a strong interaction between the river plume and the bottom, explained by the low bathymetry and by the vertical tidal mixing. Applying to a given estuary the analysis made by *Yankovsky and Chapman* [1997] for the Mekong river plume shows that in our case, the advection depth is rather shallow ($h_b \simeq 0.8$ meters during the dry season, and $h_b \simeq 1.5$ meters during the wet season). This should show that the river plume is surface advected, which proves not to be the case for mostly two reasons: the first one is that freshwater will tend to mix in one of the small bays of the Mekong delta before actually forming the coastal buoyant current (computing h_b for a bay gives $h_b \simeq 5$ meters in March, which is much closer to observations), and the second one is that the tidal mixing effects are not taken into account in the analysis of *Yankovsky and Chapman* [1997]. Although we can observe on numerical results that most of the potential vorticity brought by the freshwater inflow is actually expressed at a depth close to 5 meters, a part of non stratified plume sticks to the bottom mostly because of the vertical mixing brought by tidal currents. We can conclude from this simple analysis, that tropical rivers will have a strong tendency to form a broad coastal buoyant baroclinic current, this is explained of course by the low value of the Coriolis parameter. Except for some extreme cases like the Amazon river that is rejected almost on the Equator, the Mekong river case shows that the plume is still mostly geostrophic. This wideness and the stronger tendency to be surface advected should make the plume less sensible to the bottom friction, but the shallow areas in which tropical river plumes often flow limit this aspect and the vertical mixing generated by tidal currents has a strong impact.

[68] In our model configuration, the horizontal and vertical structures are well described, as confirmed by comparison with in situ measurements made during the months of March and October 1997. The horizontal structure defined here by the extent of the SSS anomaly is well predicted by the model as shown by comparison with measurements. The vertical structure corresponds well to the measurements, as the depth of the halocline is described with a good precision. For the month of October, some errors of sea surface salinity can be noticed, especially once the baroclinic current flows again with the coast on its right (i.e., once the upwelling event is over). The parametrization of estuaries in this paper has been based, as a first approximation, on the assumption that tidal diffusion is mostly responsible for the penetration of a salt in the estuary. Full baroclinic aspects of salt penetration in estuaries should be better taken into account in further studies. Estuarine variability must also be better taken into account and linked to forcing variability aspects more precisely (coastal ocean variability caused by wind forcing for instance).

[69] The haline vertical structure is influenced by vertical mixing caused by tidal currents. The depth of the shallow areas close to the coast can be detected in the haline structure once the plume has reached deeper locations. The shape of the haline vertical structure can be thought as being conditioned by the shallow areas in which tidal mixing may diffuse up to the surface and one can notice the presence of the halocline at a constant depth that corresponds to the depth of the shallow areas that extend off the coast.

[70] Our simulations confirm what was already suspected by *Simpson* [1997], and shown for the Amazon river by *Geyer* [1995]: tidal mixing is an important key to understand tropical river plume dynamics, because their river mouth is frequently located in shallow sedimentary plain. This is the case for the Mekong river, but also for many smaller size rivers that provide freshwater input to the continental shelf located between northern Australia and southeastern Asia. Although this flux is small for each river, the total flux it represents is important as illustrated by *Dai and Trenberth* [2002]. We can suspect this to be also true for some large tropical rivers like the Brahmaputra, the Gange and the Irrawaddy that also flow into a shallow shelf sea. For the sake of the length of this article, we have chosen not to include any sensitivity test results, meanwhile the test carried out in order to validate our tidal mixing parametrization has shown that baroclinic dynamics introduced by freshwater inflow are sensitive to this vertical mixing. Further work must be done to establish how this mixing affects fluxes of salt, freshwater, volume and momentum entering or exiting the region of freshwater influence.

[71] We have shown some important processes for tropical rivers that flow into coastal shelves regions can be parameterized for any area as they only need data accessible from global models. Our test case has been realized using a high-resolution model, but our final goal is to adapt the presented parametrizations in a configuration of lower resolution, like those used by ocean GCMs (half-a-degree resolution). It has also to be verified that the processes we have neglected for the moment are not of significant importance for a global approach or if some rivers will require a parametrizations of these processes. We intend to

progress in this direction by alternating studies with the OPA GCM and the POM regional model.

[72] **Acknowledgments.** Computational tasks for this study required the resources of the Centre de Ressources Informatiques de Haute-Normandie (CRIHAN). The authors wish to express their gratitude to the staff of the CRIHAN for its efficient contribution. Thanks to all the people that provided data for this survey: Guenter Landmann for the EU Cuu-Long project data sets that were used for comparison; Fabien Lefèvre, Maxence Revault d'Allones, and Bernard Simon for tidal harmonics; and ECMWF (Reading) for ERA40 reanalysis data. The authors wish to thank the two anonymous reviewers who helped improve this work and the present manuscript.

References

- Battisti, D. S., and A. J. Clarke (1982), A simple method of estimating barotropic tidal currents on continental margins with specific application to the M2 tide off the Atlantic and Pacific coasts of the United States, *J. Phys. Oceanogr.*, *12*, 8–16.
- Blumberg, A., and G. Mellor (1987), A description of a three dimensional coastal ocean circulation model, *Three-Dimensional Coastal Ocean Models, Coastal Estuarine Stud.*, vol. 4, edited by N. Heaps, pp. 1–16, AGU, Washington, D. C.
- Chao, S.-Y. (1988a), Wind driven motion of estuarine plumes, *J. Phys. Oceanogr.*, *18*, 1144–1166.
- Chao, S.-Y. (1988b), River forced estuarine plumes, *J. Phys. Oceanogr.*, *18*, 72–88.
- Chao, S.-Y., and W. C. Boicourt (1986), Onset on estuarine plumes, *J. Phys. Oceanogr.*, *16*, 2137–2149.
- Cook, T. M. (2000), Surface tidal current variability on the North Carolina shelf observed with high frequency radar, M.S. thesis, Rosenstiel School of Mar. and Atmos. Sci., Univ. of Miami, Miami, Fla.
- Dai, A., and K. Trenberth (2002), Estimates of freshwater discharge from continents: Latitudinal and seasonal variations, *J. Hydrometeorol.*, *3*, 660–687.
- Flather, R. (1976), A tidal model of the north-west European continental shelf, *Mem. R. Sci. Soc. Liège*, *10*, 141–164.
- Fong, D., and W. Geyer (2001), Response of a river plume during an upwelling favorable wind event, *J. Geophys. Res.*, *106*, 1067–1084.
- Fong, D., and W. Geyer (2002), The alongshore transport of freshwater in a surface-trapped river plume, *J. Phys. Oceanogr.*, *32*, 957–972.
- Fong, D., W. Geyer, and R. Signell (1997), The wind-forced response on a buoyant coastal current: Observations of the western Gulf of Maine, *J. Mar. Syst.*, *12*, 69–81.
- García Berdeal, I., B. M. Hickey, and M. Kawase (2002), Influence of wind stress and ambient flow on a high discharge river plume, *J. Geophys. Res.*, *107*(C9), 3130, doi:10.1029/2001JC000932.
- Garratt, J. (1977), Review of drag coefficients over oceans and continents, *Mon. Weather Rev.*, *105*, 915–929.
- Garvine, R. (1995), A dynamical system for classifying buoyant coastal discharges, *Cont. Shelf Res.*, *15*, 1585–1596.
- Garvine, R. (1999), Penetration of buoyant coastal discharge onto the continental shelf: A numerical model experiment, *J. Phys. Oceanogr.*, *29*, 1892–1909.
- Geyer, W. (1995), Tide-induced mixing in the Amazon frontal zone, *J. Geophys. Res.*, *100*, 2341–2353.
- Geyer, W., and G. Kineke (1995), Observations of currents and water properties in the Amazon frontal zone, *J. Geophys. Res.*, *100*, 2321–2339.
- Geyer, W., R. Beardsley, S. Lentz, J. Candela, R. Limeburner, W. Johns, B. Castro, and I. Soares (1996), Physical oceanography of the Amazon shelf, *Cont. Shelf Res.*, *16*, 575–616.
- Geyer, W., P. Hill, T. Milligan, and P. Traykovski (2000), The structure of the Eel river plume during floods, *Cont. Shelf Res.*, *20*, 2067–2093.
- Hetland, R. D. (2005), Relating river plume structure to vertical mixing, *J. Phys. Oceanogr.*, *35*, 1667–1687.
- Hungspreugs, M. (Ed.) (1998), *Proceedings of the International Workshop on the Mekong Delta*, Cuu Long Proj., Eur. Comm., Brussels.
- Kourafalou, V., T. Lee, L.-Y. Oey, and J. Wang (1996a), The fate of river discharge on the continental shelf: 2. Transport of coastal low-salinity waters under realistic wind and tidal forcing, *J. Geophys. Res.*, *101*, 3435–3455.
- Kourafalou, V., L.-Y. Oey, J. Wang, and T. Lee (1996b), The fate of river discharge on the continental shelf: 1. Modeling the river plume and the inner shelf coastal current, *J. Geophys. Res.*, *101*, 3415–3434.
- Landmann, G., V. Hutflits, F. Hagemann, and V. Ittekkot (1998), Distribution and behaviour of suspended matter and sediments in the Mekong River and adjacent sea, in *Proceedings of the International Workshop on the Mekong Delta*, pp. 100–105, Cuu Long Proj., Eur. Comm., Brussels.
- Lentz, S., M. Carr, and T. Herbers (2001), Barotropic tides on the North Carolina shelf, *J. Phys. Oceanogr.*, *31*, 1843–1859.
- Levitus, S., R. Burgett, and T. P. Boyer (1994), *World Ocean Atlas 1994*, vol. 3, *Salinity, NOAA Atlas NESDIS*, vol. 3, 111 pp., U.S. Gov. Print Off., Washington, D.C.
- MacCready, P. (1999), Estuarine adjustment to changes in river flow and tidal mixing, *J. Phys. Oceanogr.*, *29*, 708–726.
- MacCready, P. (2004), Toward a unified theory of tidally-averaged estuarine salinity structure, *Estuaries*, *27*, 561–570.
- Madec, G., P. Delecluse, M. Imbard, and C. Levy (1998), Opa 8.1, ocean general circulation model, *Note Pole Model. 11*, 91 pp., Inst. Pierre-Simon Laplace, Paris.
- Marsaleix, P., C. Estournel, V. Kondrachoff, and R. Vehil (1998), A numerical study of the formation the Rhone river plume, *J. Mar. Syst.*, *14*, 99–115.
- Masse, A. K., and C. Murphy (1990), Observations of the Niagara river plume, *J. Geophys. Res.*, *95*, 16,097–16,109.
- Mellor, G. (2002), Oscillatory bottom boundary layers, *J. Phys. Oceanogr.*, *32*, 3075–3088.
- Mellor, G., and T. Yamada (1982), Development of a turbulence closure model for geophysical fluid problems, *Rev. Geophys.*, *20*, 851–875.
- Monismith, S. G., W. Kimmerer, J. R. Burau, and M. T. Stacey (2002), Structure and flow-induced variability of the subtidal salinity field in northern San Francisco Bay, *J. Phys. Oceanogr.*, *32*, 3003–3019.
- Münchow, A., and R. Garvine (1993), Buoyancy and wind forcing of a coastal current, *J. Mar. Res.*, *51*, 293–322.
- Munk, W., and C. Wunsch (1998), Abyssal recipes ii: Energetics of tidal and wind mixing, *Deep Sea Res., Part I*, *45*, 1977–2010.
- Ngo-Duc, T., J. Polcher, and K. Laval (2005), A 53 year forcing data set for land-surface models, *J. Geophys. Res.*, *110*, D06116, doi:10.1029/2004JD005434.
- O'Donnel, J. (1990), The formation and fate of a river plume: A numerical model, *J. Phys. Oceanogr.*, *20*, 551–569.
- Oey, L.-Y., and G. Mellor (1993), Subtidal variability of estuarine, plume and coastal current: A model study, *J. Phys. Oceanogr.*, *23*, 164–171.
- Ramette, M. (1981), Guide d'hydraulique fluviale, *Rep. HE40/81.04*, Lab. Natl. d'Hydraul., Chatou, France.
- Rippeth, T. P., E. Williams, and J. H. Simpson (2002), Reynolds stress and turbulent energy production in a tidal channel, *J. Phys. Oceanogr.*, *32*, 1242–1251.
- Simpson, J. (1997), Physical processes in the Rofi Regime, *J. Mar. Syst.*, *12*, 3–15.
- Simpson, J., and J. Hunter (1974), Fronts in the Irish Sea, *Nature*, *250*, 404–406.
- Simpson, J., and A. Snidvongs (1998), The influence of monsoonal river discharge on tropical shelf seas: The Gulf of Thailand as a case for study?, in *Proceedings of the International Workshop on the Mekong Delta*, pp. 86–99, Cuu Long Project, Eur. Comm., Brussels.
- Smagorinsky, J. (1963), General circulation experiments with primitive equations, 1. The basic experiment, *Mon. Weather Rev.*, *91*, 99–164.
- Smolarkiewicz, P. K. (1984), A fully multidimensional positive definite advection transport algorithm with small implicit diffusion, *J. Comput. Phys.*, *54*, 325–362.
- Weaver, A.-J., and W. Hsieh (1987), The influence of buoyancy flux from estuaries on continental shelf circulation, *J. Phys. Oceanogr.*, *17*, 2127–2140.
- Yankovsky, A. (2000), The cyclonic turning and propagation of buoyant coastal discharge along the shelf, *J. Mar. Res.*, *58*, 585–607.
- Yankovsky, A., and D. Chapman (1997), A simple theory for the fate of buoyant coastal discharges, *J. Phys. Oceanogr.*, *27*, 1386–1401.
- Yankovsky, A., B. Hickey, and A. Munchow (2001), Impact of variable inflow on the dynamics of a coastal buoyant plume, *J. Geophys. Res.*, *106*, 19,809–19,824.

R. Hordoir (corresponding author) and K. D. Nguyen, Laboratoire de Morphodynamique Continentale et Côtière, 2-4 rue des Tilleuls, F-14000 Caen, France. (hordoir@meca.unicaen.fr)
J. Polcher, Laboratoire de Météorologie Dynamique du CNRS, IPSL, CNRS, F-75252 Paris, France.